DEVELOPMENT AND VALIDATION OF MECHANICAL PROPERTIES MODELS FOR DP STEELS

J. H. Bianchi and P. Vescovo

Centro Sviluppo Materiali SpA, Via di Castel Romano 100, 00128 Roma, Italy

Keywords: Dual phase steels, Self Consistent Strain, multiphase properties, size effects

Abstract

This experimental-modelling work aimed to gain a better understanding of and to quantify the effect of complex microstructure parameters on the mechanical properties of Dual Phase steels (DP).

Mixed Ferrite-Martensite (F-M) structures have been produced from a hot rolled Ferrite-Pearlite steel by combination of reheating-quenching cycles for grain refinement followed by intercritical annealing in the range 720 ℃ to 815 ℃. The final microstructures have been characterised by optical microscopy, revealing M contents ranging from 2 to 16%, mean Ferrite grain sizes (FGS) from 9 to 22 microns and Martensite equivalent mean diameters d_M from 0.6 to 2.9 microns. Tensile testing on cylindrical specimens at quasi-static conditions and strain rates up to five orders higher have been performed for both quantification of stress sensitivity to strain rate and validation of the simulations.

The simplest empirical models for *engineering tensile parameters* obtained from the experiments show that strength Rm, strain to fracture and toughness have sensitivity to d_M almost one order of magnitude higher than to FGS. The Rm sensitivity to percentage M-content is about half of its value to d_M in microns. The higher strength to yield stress ratios correspond to the smallest structural sizes and to lowest M-contents.

Two constitutive models for *hardening characteristics* of multiphase steels have also been developed. The **SCS-m** is a Self-Consistent Strain formulation model allowing strain partition between phases and valid up to the uniform deformation limit. The **MS-m** is a Multiphase Strain model incorporating damage and applicable up to near fracture. Both models have been interfaced to a FEM platform, in view of their potential extension to cold forming and dynamic loading end-user applications. The simulation results have been extensively validated in a wide span of strain rate and M-contents, and up to very large strains past the onset of tensile necking. A measure of tensile toughness obtained from the simulations has been correlated to microstructural parameters.

1 Introduction

The simplest approach to model tensile properties of multiphase steels is to correlate experimental and microstructural parameters and many expressions of this type have been proposed [1-3]. The more elaborated modelling approaches for simulation of hardening characteristics in a wide strain range can be divided in two main groups:

Micro-FEM discrete models that mesh representative metallurgical structures and assign distinctive constitutive behaviour to each phase [2, 3]. The Strain Gradient Plasticity formulation [4] used in [3] is particularly interesting because the built up of dislocation density at grain boundaries results naturally from the formulation. It has successfully reproduced Hall-Petch relationships without making any assumption on the effects of grain size or assigning additional properties to grain boundaries. The handicap of this type of modelling is the intensive work required to mesh intricate real metallurgical structures, but some simplifications (Wojcicki in [2]) have allowed studying the influence of size and distribution of Martensite clusters in three dimensions.

Continuous models that assume homogeneously distributed phases are by far easier to implement and use. They vary from plain empirical models based on the measured macroscopic strain, models incorporating M-induced Ferrite strengthening [5-6] but still based on the dual phase total strain and models discriminating the different deformation of each phase on hypothesis of iso-Work [7] and Self-Consistent Strain (**SCS-m**) [8-12]. The last type of modelling requires the input of single-phase constitutive laws and has been applied in the past using either literature expressions or extrapolating data from structures already multiphase to obtain the properties of single constituents [11-12]. The performance of these multiphase models is reviewed in the current work using recent improved constitutive equations for single phases, which have a yield stress related to chemical composition and a strain hardening driven by mean free path parameters [1,2]. The

work led to quantification of an additional hardening in Ferrite due to M-presence.

Several F-M structures have been experimentally produced from a combination of reheating-quenching cycles and intercritical annealing. The materials were tested at quasi-static conditions and up to 4 s^{-1} strain rates and their results used to produce both empirical relationships for single tensile parameters and for development and validation of the **SCS-m** and **MS-m** models describing the work hardening characteristics.

2 Experimental

The original material was a Ferrite-Pearlite hot rolled 16 mm thickness plate with the composition in Table 1. The coarse structure was refined by different reheating and quenching treatments, and several DP structures were subsequently obtained by intercritical annealing. The aim of this work was to obtain a variety of M-content and DP parameters. Table 2 shows the matrix of thermal treatments, carried on bars of 130 mm x 16 mm x 16 mm cut to nearly the final size for the mechanical testing specimens. Temperature and cooling rates were measured using a thermocouple embedded in the specimen.

Two types of thermal treatments were investigated. In the first set, intercritical annealing at the two fixed temperatures of 740 ℃ and 760 ℃ were used f or a variety of pre-refined structures (CA-CF, Table 2). In the second set, the starting structure was fixed (CF) and intercritical annealing at 6 temperatures in the range from 720 ℃ to 816 ℃ wer e made. All structures were quenched in ice-cooled water after treatment.

C	Mn	Si	Cr	Ni	Cu	Mo	N	Al	P	Nb, Ti, V
0.1	1.10	0.10	0.20	0.10	0.14	0.21	<0.01	0.03	0.003	< 0.005

Table 1: Chemical composition (mass %)

ANNEALING	STRUCTURE REFINEMENT																							
	CA				CB				CC				CD				CE				CF			
	as hot rolled				CA + (56') at 880℃ + W.Q. + 120' at 550℃+ W.Q.				CA + (56') at 880 ℃ + A.C.				CC + (55') at 870 ℃ + W.Q.				CD + (55') at 870 ℃ + A.C.				CD+(55') at 870 ℃ + W.Q. + (55') at 870 ℃ +A.C.			
	T_H	t_R	t_H	CR	T_H	t_R	t_H	CR	T_H	t_R	t_H	CR	T_H	t_R	t_H	CR	T_H	t_R	t_H	CR	T_H	t_R	t_H	CR
1																					721	29	20	19
2																					731	23	27	31
3	741	38	14	18	741	23	23	18	741	38	14	18	741	38	14	18	741	23	23	18	743	23	13	76
4	761	31	12	25	761	36	15	61	761	31	12	25	759	34	16	16	759	34	16	16	761	38	15	82
5																					782	20	20	141
6																					816	20	14	31

Table 2: Structure refinement and intercritical annealing conditions used to modify the original F-P steel; t_R= time to reach the holding temperature [min]; T_H=Holding Temperature [℃]; t_H =holding time [min]; CR=cooling rate [℃/s]; A.C.=air cooling; W. Q.=water cooling.

ID	Nital	Sodium Meta bi-Sulphide	Le-Perà		
	Mean F.G.S. D $[\mu m]$, <std>	$M[\%]$	$M[\%]$, <std %>	Roundness ratio, <std>	Equivalent mean diameter from area $d_M[\mu m]$, <std>
CA3	12.6, <3.4>		7.9, <0.42>	1.40, <0.39>	1.71, <0.57>
CB3	9.2, <3.3>		8.9, <0.38>	1.29, <0.32>	1.46, <0.45>
CC3	22.4, <3.5>		9.1, <0.44>	1.80, <0.49>	2.88, <0.71>
CD3	7.9, <2.9>		9.3, <0.40>	1.32, <0.35>	1.54, <0.48>
CE3	9.4, <3.2>		9.2, <0.39>	1.38, <0.37>	1.85, <0.55>
CF1	14.0, <3.5>	1.8	1.9, <0.24%>	1.028, <0.06>	0.93, <0.16>
CF2	11.3, <2.0>	2.9	3.8, <0.26%>	1.028, <0.04>	1.23, <0.21>
CF3	13.0, <2.3>	8.4	10.5, <0.55%>	1.045, <0.06>	1.27, <0.22>
CF4	10.7, <2.0>	10.5	10.8, <0.90%>	1.032, <0.05>	1.39, <0.20>
CF5	13.7, <2.9>	10.3	15.7, <0.96%>	1.027, <0.04>	1.36, <0.21>
CF6	10.6, <3.4>	10.8	10.6, <0.39%>	1.032, <0.05>	1.25, <0.23>

Table 3: Metallurgical parameters of the DP microstructures studied; <std>= standard deviation

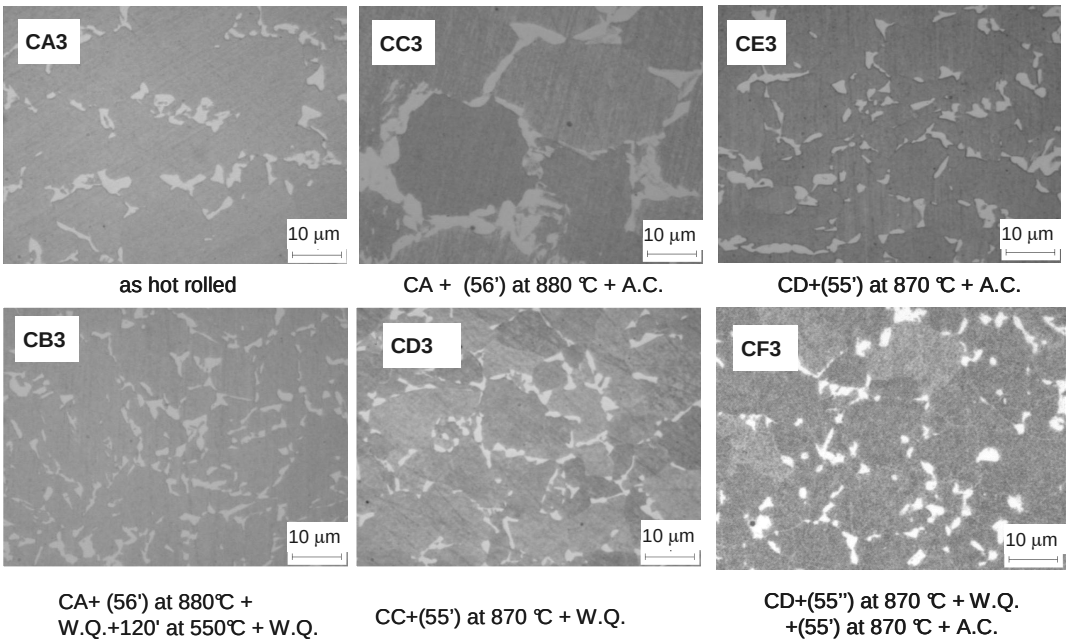

Figure 1: Effect of the refining structure pre-treatment on the microstructures subsequently produced by intercritical annealing at 740 ℃. Le- Perà etching.

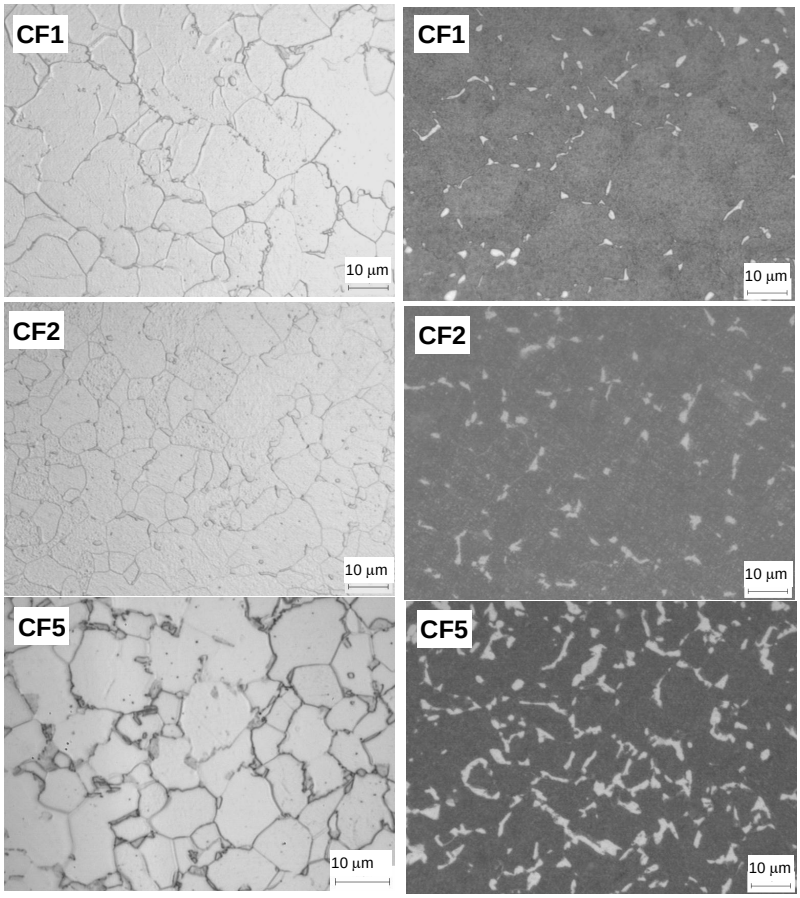

Figure 2: Effect of the intercritical annealing temperature on microstructures obtained from a common refinement pre-treatment. Left: Nital 4% etching, right: Le-Pera etching. Annealing temperatures: CF1=720 ℃, CF2=730 ℃, CF5=780 ℃.

Figure 1 and Table 3 show the effects of varying the refining pre-treatment conditions on the microstructures obtained after the subsequent intercritical annealing at a common 740 ℃ temperature. They have a mean FGS varying from 9.2 to 22.4 microns, M-content 8-9% and d_M from 1.5 to 2.9 microns. The coarser structure was obtained by only one refinement ended in air cooling (CC3).

Figure 2 and Table 3 show the effect of the annealing temperature on the common pre-treated structure CF. The mean FGS varies between 10.6 and 14 microns and does not show a definite trend with either the holding temperature, time or cooling rate. A small amount of Bainite, estimated in 2-3% for the CF1-CF5 samples and slightly higher in CF6 was observed. Martensite contents varying from 1.9 to 15.8 % and d_M 0.9 to 1.4 microns were obtained.

Cylindrical specimens of 9 mm gauge diameter were machined from the heat treated bars for tensile testing at speeds from 0.00024 s^{-1} to 4 s^{-1}.

3 Modelling Quasi-Static tensile testing

3.1 Empirical models for engineering parameters

The experimental tensile testing parameters have shown clear correlations in terms of:

(a) *M-content:* Rm increases at a rate of 7 [MPa / %M] (Figure 3). Rp02 is not sensitive to M below 3.8% and then increases at 4 [MPa / %M]. The strength/yield ratio Rm/Rp02 decreases at -0.018 [1/% M]. The uniform strain decreases with the M-fraction at a ratio -0.0026 [1 / %M] while a strain to fracture computed from the area reduction of broken specimens shows a large drop from 1.8 for the 1.9% M, to around 1.22 for all the higher M-contents. The higher strain to fracture resulted for the specimens annealed from the as-hot rolled plate (CA3) and from the refinement ending in air cooling (CE3), but this lowered Rm. A linear trend with gain of uniform strain achieved at expense of dropping the tensile strength for decreasing M-contents was found.

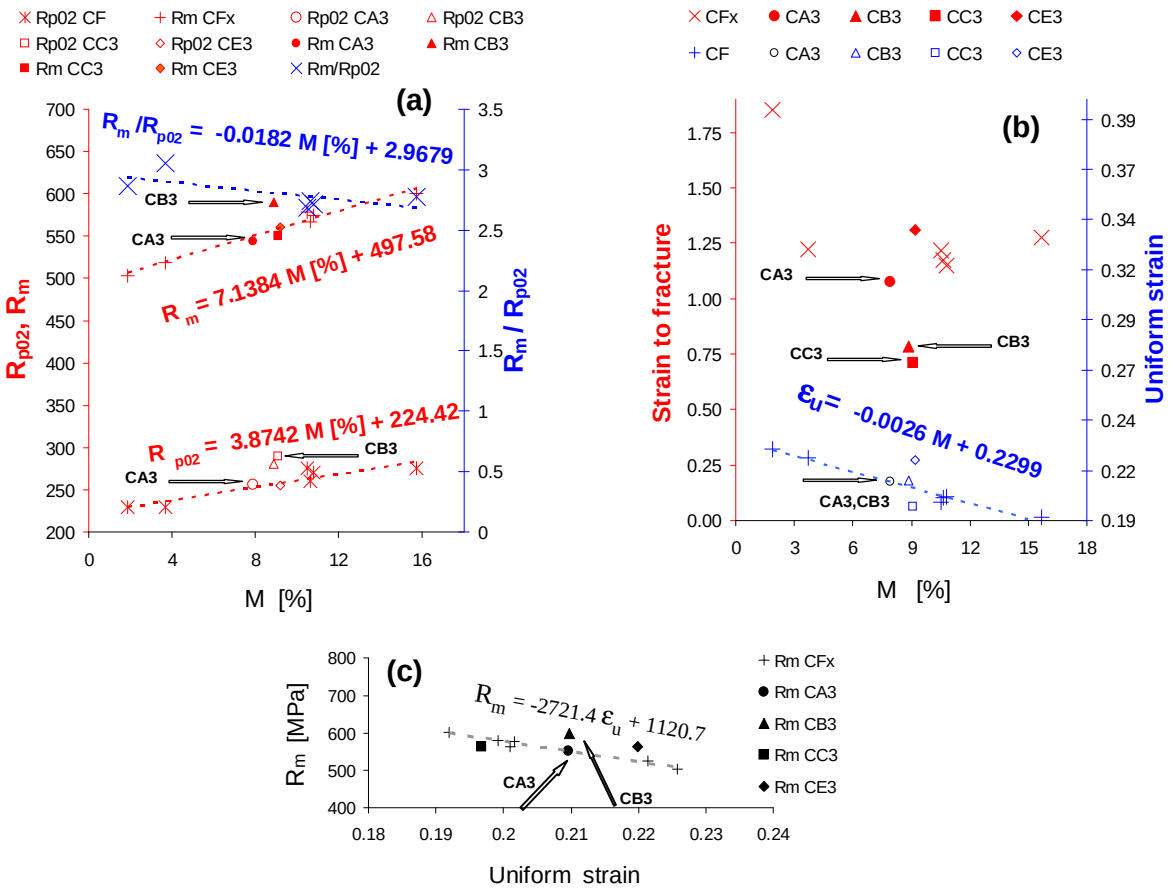

Figure 3: Effect of M-content on the main tensile parameters: (a) strength; (b) strains; (c) compromise strength-ductility. 9 mm diameter specimens, quasi-static strain rate. Strain to fracture computed as $\Delta A/A$ with A= fracture area.

(b) *Phase mean sizes*: The results for the Cx3 samples intercritically annealed at 740 ℃ show that Rm decreases at a rate (-1.6 MPa/microns) with the mean FGS and almost one order of magnitude faster (-15 MPa/microns) with d_M (Figure 4). Rp02 increases as the structure is coarser, at a faster rate with d_M (11 MPa/microns) than with the FGS (2.3 MPa/microns). The Rm/Rp02 ratio decreases with the increase of structural dimensions, at –0.0223 MPa/microns with FGS and at –0.13 MPa/microns with d_M .

The fracture strain decreases with the increase of microstructure dimensions and is almost one order of magnitude more sensitive to d_M (-0.27 MPa/microns) than to FGS (-0.04 MPa/microns). The uniform strain is also more sensitive to d_M than to FGS, both values being low but representing however about a 10% total variation for the range of sizes examined.

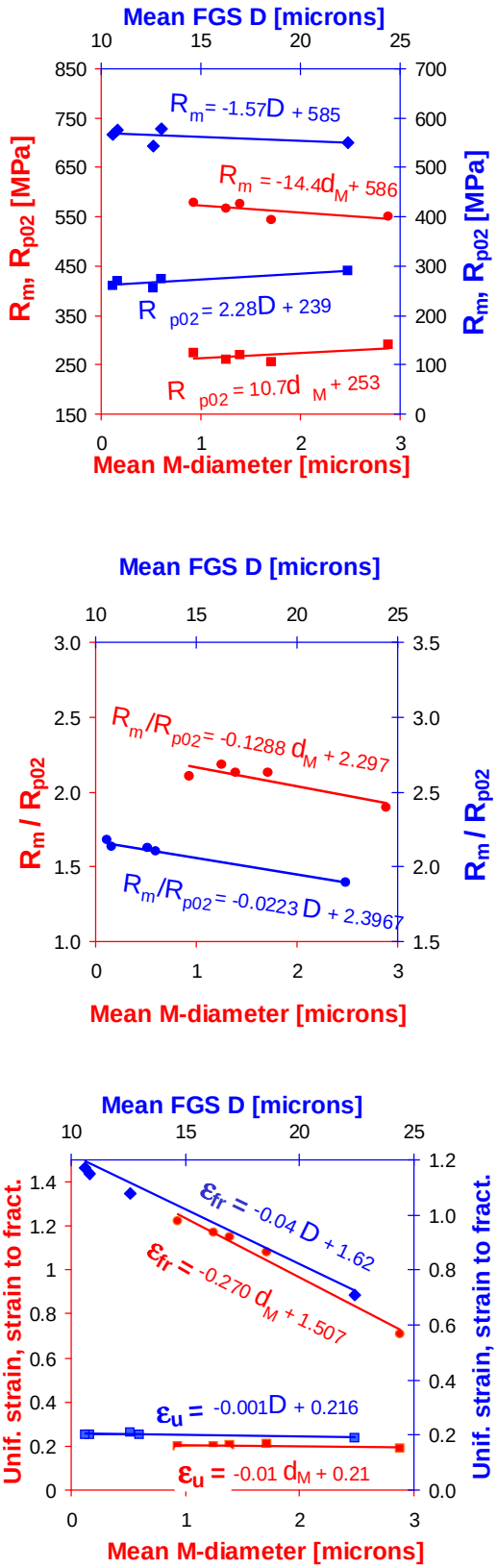

Figure 4: Effect of metallurgical parameters on the quasistatic tensile properties of a 11% M DP steel.

The results show that tensile properties are more influenced by the d_M size in microns (Figure 4) than by the percentage M-volume fraction (Figure 3). The sensitivity of Rm to percentage M-content is half than to d_M in microns.

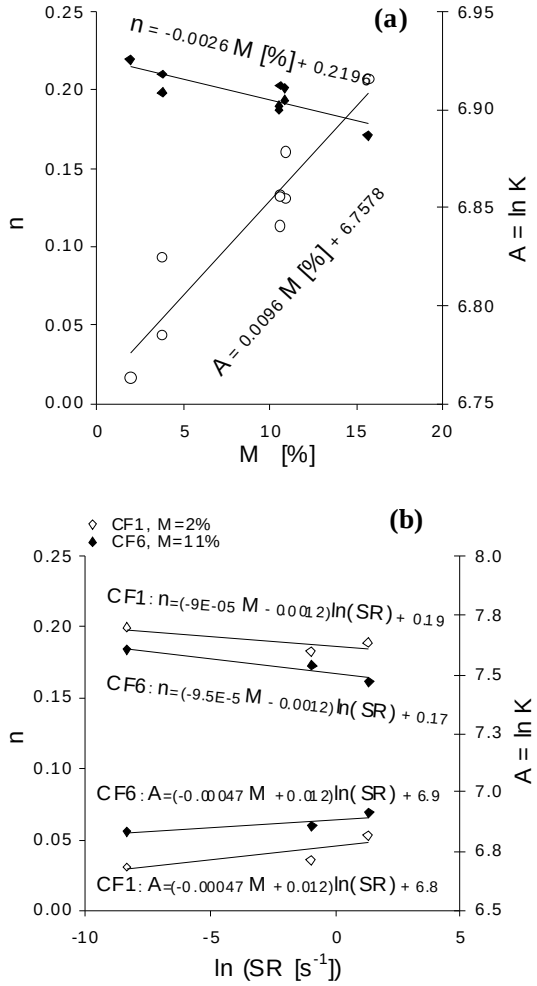

Figure 5: Effects on the constitutive coefficients in $\sigma = K(\varepsilon - \varepsilon_o)^n$ of: (a) M-content at the quasistatic strain rate; (b) strain rate and M-content.

Each experimental stress-strain curve was next fitted by the Swift law: $\sigma = K(\varepsilon - \varepsilon_o)^n$ in terms of the macroscopic strain, leaving as free parameters the stress factor K and the strain hardening coefficient n. A subsequent analysis of these two parameters in the range 2-16 %M shows that n varies in about 20% at a ratio -0.0026 [1/ M%] (Figure 5a) whilst the K total variation is 12 % increasing at 0.0096 [MPa/%M]. These results in terms of the multiphase strain, are used in the MS-m model detailed in Table 4.

3.2 Self-Consistent Strain model for strain hardening characteristics

The **SCS-m** was developed upon an earlier Base Self-Consistent Strain FEM model (T4.2 in Table 4) [11-12], in which the strain-rate partition ratio formulation of Stringfellows *et al* [8] was modified in terms of strain increments similarly to Tomota *et al.* [9-10] and implemented as a user-defined Elastoplastic model interfaced to a commercial FEM code [14]. The model assumes uniformly distributed phases, each of which takes a strain according to its strength. Single constituent strain-stress curves were computed from the chemical composition and parameters in Tables 1 and 3, using expressions taken from literature for pure Ferrite (T4.1 in Table 4, [1]) and modified strength for pure Martensite accordingly to the recent findings of Gutierrez in [2]. The strain hardening in these expressions is defined in terms of a mean free-path dimensions taken as the FGS for Ferrite and the lath dimension for Martensite. The predictions of this Base SCS model underestimate the experimental data (Figure 6), with a difference in the macroscopic true-stress:

$$\Delta\sigma = \sigma^{experimental} - \sigma^{FEM \quad Base\ SCS\ model} \tag{1}$$

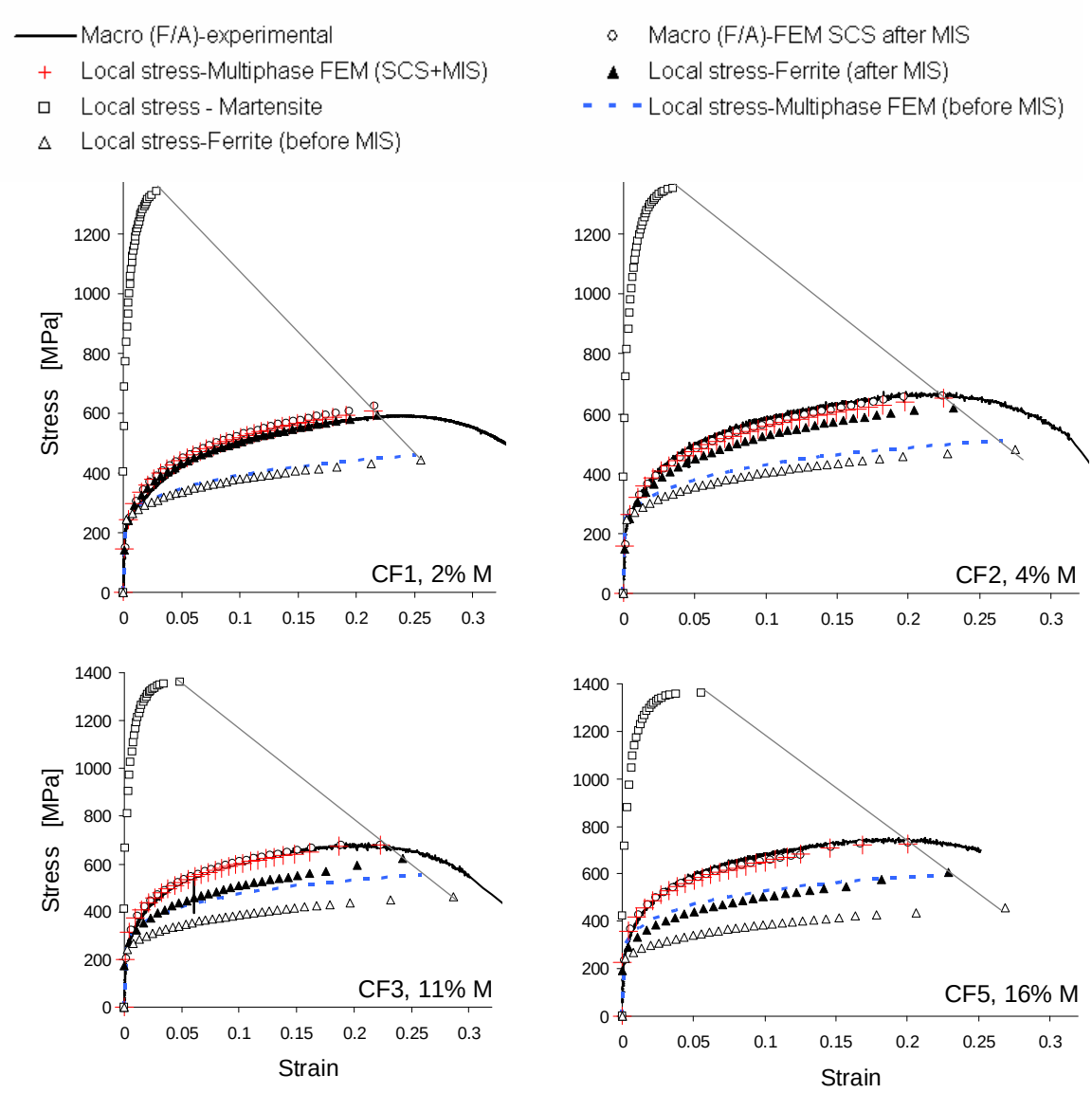

Figure 6: Comparison of experimental and SCS-m simulation results for series CF. Both macroscopic and local simulation results are shown, the last with and without the MIS correction.

SCSm

QS: strength of single phases [1]:

$$\sigma_F = \sigma_{oF} + B_F \cdot F(\varepsilon_F), \qquad \sigma_M = \sigma_{oM} + B_M \cdot F(\varepsilon_M) \qquad \text{(T4.1)}$$

$$\sigma_{oF} = 77 + 80\cdot\%Mn + 750\cdot\%P + 60\cdot\%Si + 80\cdot\%Cu + 45\cdot\%Ni + 60\cdot\%Cr + 11\cdot\%Mo + 5000\cdot N_{ss} + 5000\cdot C_{ss}$$

$$\sigma_{oM} = 77 + 80\cdot\%Mn + 750\cdot\%P + 60\cdot\%Si + 80\cdot\%Cu + 45\cdot\%Ni + 60\cdot\%Cr + 11\cdot\%Mo + \Delta\sigma_c$$

$$B_{F,M} = \alpha \cdot M \cdot \mu \cdot \sqrt{b}\ , \quad \alpha = 0.33\ , \quad M = 3\ , \quad \mu = 82400\ \text{[MPa]}, \quad b = 2.48.10^{-10}\ \ [m]$$

$$F(\varepsilon) = \sqrt{\frac{1 - e^{-C\,\varepsilon}}{E}}\ , \qquad C_{F,M} = M \cdot k_{F,M}\ , \qquad E_F = k_F\,.(FGS) \qquad k_F = 1.4$$

Model M-1.1[1]: $E_M = k_M . L_M$, $\Delta\sigma_C = 3065\cdot\%C - 161\text{[MPa]}$, $k_M = 38$, $L_M = 0.035\mu m$

Model M-1.2, Gutierrez in [2] : $F(\varepsilon) = A\ \frac{k_1}{k_2}\left[1 - \left(1 - \frac{k_2}{k_1} b\sqrt{\rho_o}\right)\cdot e^{-\frac{k_2 M \varepsilon}{2}}\right], \quad \Delta\sigma_C = 0$

$$k_1 = 1.69\cdot 10^{-7}\cdot\sqrt{\rho_o} - 4.52\ , \qquad k_2 = 69.81\cdot k_1^{\,0.7}$$

$$\log(\rho_o) = 8.9372 + \frac{6880.93}{M_S} - \frac{1780360}{M_S^{\,2}}, \qquad A = 1/\sqrt{b}$$

QS: Base Self Consistent Strain FEM model (Bianchi *et al* in [11,12]) (T4.2)

Input: f_M, *single phase constitutive laws from* (T4.1): $\sigma_F(\varepsilon_F)$ *and* $\sigma_M(\varepsilon_M)$

Output: *Phase strains*: $\varepsilon_F, \varepsilon_M$, *composite strain and stress* ε, σ_{QS}

QS: SCS with Multiphase-Interaction Stress in Ferrite (SCS + MIS) FEM model (T4.3)

The Base SCS model in (T4.2) is applied modifying the ferrite strength as:

$$\sigma_F(\varepsilon_F) \ \textit{single phase constitutive law} \ + \ \Delta\sigma\left(\varepsilon_{multiphase}, f_M, d_M, D\right)$$

RD: Rate-Dependent Plasticity, SCS-m FEM model. (T4.4)

The (SCS + MIS) model in (T4.3) is applied modifying the Ferrite strength as:

$$\sigma_{F,RD}(\dot\varepsilon) = \sigma_{F,QS}(\dot\varepsilon_o)\ .\ k(\varepsilon\ , \dot\varepsilon) \qquad \text{with:} \qquad k(\varepsilon_F, \dot\varepsilon_F) = \varepsilon_F^{\,-0.0012\ln\left(\dot\varepsilon/\dot\varepsilon_o\right)}\ .\ e^{0.01229\ ln(\dot\varepsilon/\dot\varepsilon_o)}$$

MSm

RD-Rate-dependent Plasticity, FEM model (T4.5)

$$\sigma_{RD}(\dot\varepsilon) = \sigma_{QS}(\dot\varepsilon_o).\ k(\varepsilon, \dot\varepsilon, M[\%]) \quad \text{with:} \quad \sigma_{QS}(\dot\varepsilon_o) = \varepsilon^{-0.0026\,\mathrm{M}[\%] + 0.2196}\ .\ e^{0.0096\,\mathrm{M}[\%] + 6.7578} \text{ and:}$$

$$k(\varepsilon, \dot\varepsilon, M[\%]) = \varepsilon^{(-0.00009\cdot M[\%] - 0.0012)\ln\left(\dot\varepsilon/\dot\varepsilon_o\right)}\cdot e^{(-0.00047\cdot M[\%] + 0.01229)\ln\left(\dot\varepsilon/\dot\varepsilon_o\right)}$$

Material damage (Gurson FEM model) [13-14] (T4.6)

$$\sigma_{damaged} = (1 - f)\sigma \qquad \text{with:}$$

$$\dot f = \dot f_{gr} + \dot f_{nucl.}\ , \qquad \dot f_{gr} = (1 - f)\dot\varepsilon_{volumetric}\ , \qquad \dot f_{nucl.} = A\ \dot\varepsilon_N \quad \text{and} \quad A = \frac{f_N}{s_N\sqrt{2\pi}}\exp\left[-0.5\left(\frac{\varepsilon - \varepsilon_N}{s_N}\right)^2\right]$$

Table 4. Summary of the material models; QS=quasi-static conditions, RD= rate-dependent.

The following trends have been identified for the stress gap $\Delta\sigma$ in (1):

(a) $\Delta\sigma$ increases with the multiphase strain (Figure 7a). In spite of the differences in M-content for the CF1-CF5 specimens, all $\Delta\sigma$ results are bounded in a band about 70 MPa wide.

(b) For the CF's samples CF2-CF5 (4-16% M-content and FGS order 9-14 microns), the magnitude of the $\Delta\sigma$ correction to match the experimental values is higher but of the order that would be required by applying Bouaziz *et al* model [5] in terms of the DP total strain (Figure 7b). It is interesting to note that the work in [5] was calibrated on DPs having half FGS than in the current work, a higher M range (11-40%), and that the $\Delta\sigma$ difference found here diminishes with the FGS (Figure 7a)

(c) Two constitutive expressions for Martensite strength [1-2] with several Carbon contents were examined (T4.1 in Table 4). These ranged from C-nominal, C by applying law of mixtures and C after new M formation. The difference in strength resulting from these several hypotheses had a minimal influence on the multiphase results [2], which is attributed to the low strain partition taken by Martensite (Figure 6) producing small variations of multiphase stress.

(d) The following results are apparent:

(d1) The sensitivity of $\Delta\sigma$ to the M-content is important at yield strains (2.6 [MPa/%M]) but is significantly reduced to 0.4-0.6 [MPa/%M] at tensile strains 0.20-0.15 (Figure 8a). For M > 4% and multiphase strain > 0.15, $\Delta\sigma$ values are 137-148 MPa higher than for the pure ferrite condition ($\Delta\sigma$ = 0), representing a strength increase of 22% to 24% with low influence of the M-content in the range examined.

(d2) $\Delta\sigma$ increases with the FGS (Figure 7a and Figure 8c) in 4.2 to 5.7 [MPa/microns], level which raises with the multiphase strain.

(d3) $\Delta\sigma$ increases with d_M in 15 to 21 [MPa/microns] which is four times higher than with the FGS (Figure 8b).

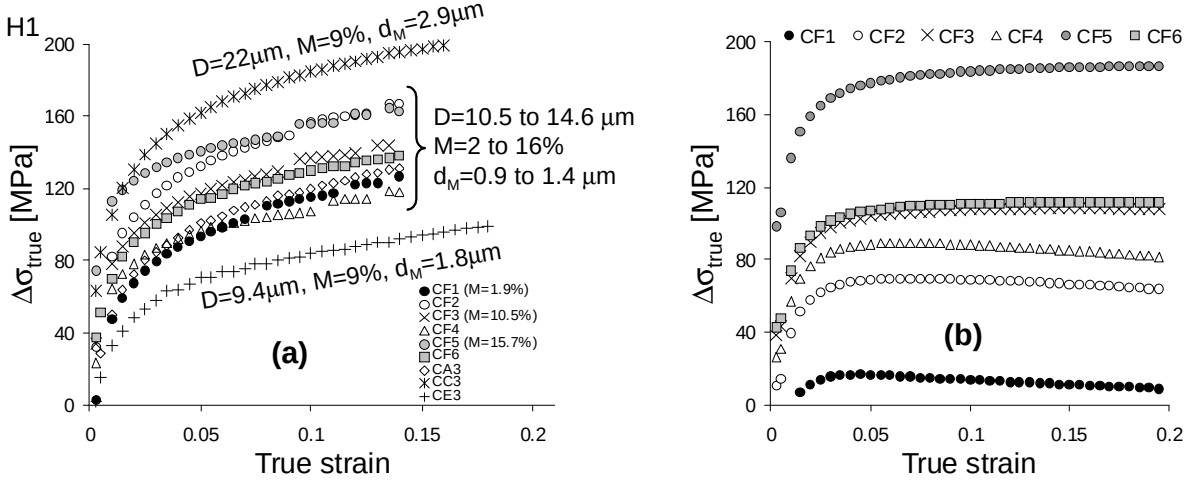

Figure 7: Comparison of the stress difference between experiments and (a) SCS-m simulations (Base SCS model with data for pure ferrite); (b) Simulations applying Bouaziz et al (2001) DP model.

Given the magnitude of the stress mismatch in equation (1) and due to the large strain taken by the matrix, the results indicate the deterioration of Ferrite strain hardening predictions based on FGS as mean free-path parameter, when M is present. Also, the low Bainite content of the CF's steels studied does not justify the significant departure of the strain-stress experimental data from the Base **SCS-m** prediction computed with pure Ferrite data. The results above suggest that a 'Multiphase Interaction Stress' (MIS) of magnitude $\Delta\sigma$, not considered in the original Base SCS model [11-12] with pure Ferrite, develops as straining starts (Figure 7). Such stress difference does not appear to be only an initial boundary condition from the Ferrite Martensite mixture around the M-islands, but the result of both strain hardening controlled by the high dislocation density in this

layer [15] and probably the growth of this. The result quoted in (d3) above support this last hypothesis, with $\Delta\sigma$ more related to the d_M (hence area of the F-M inter-phase accommodating strains layer) than to FGS and in all cases increasing with strain. Because most of the hardening is taken by the matrix, the MIS term has been incorporated in this work into the Ferrite constitutive law in terms of the composite strain, and then the multiphase behaviour determined by applying the Self-Consistent strain formulation (T4.3 Table 4).

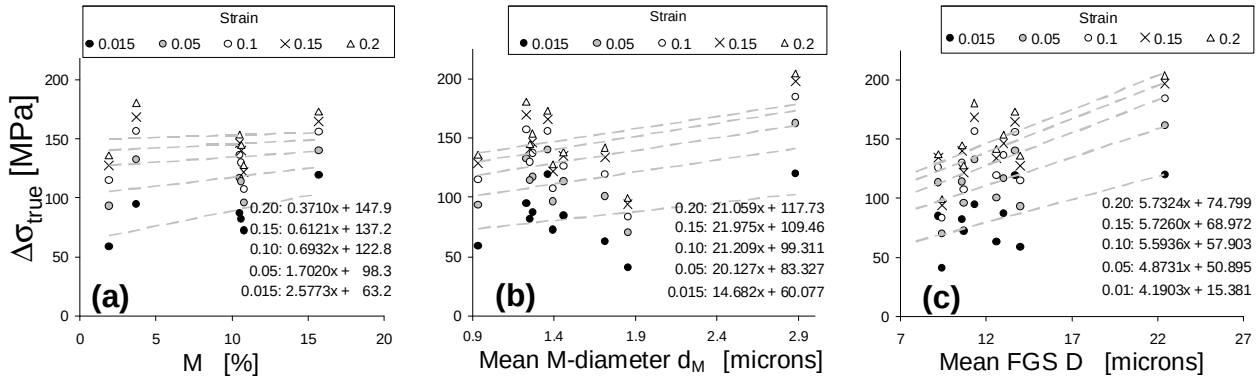

Figure 8: Dependence of the stress difference between experiments and Base SCS-m simulations using data for pure ferrite with:(a) M-content; (b) mean M-diameter; (c) mean FGS.

Both the macroscopic and local stress-strain results in Figure 6 produced with the resulting modified **SCS-m** model are in satisfactory agreement with experimental data up to the uniform strain limit. The ratio of F/M strains at the uniform strain limit is about 9.7 for 2 to 4 % M but drops to 5 for the 10%-16% M-contents.

Although the multiphase strengthening due to intrinsic M-hardening cannot be separated from the effect of M on the surrounding Ferrite matrix by experimental means, it can however be quantified by the simulations by switching on and off the $\Delta\sigma$ term. A comparison of the local strength for pure Ferrite and its associated multiphase strength without MIS correction (Figure 6), represents the gain over pure Ferrite achieved by only M-hardening and this varies from 12 MPa for the 2% M-content to 150 MPa for the 16 % M. In contrast, the effect of Martensite on surrounding Ferrite (MIS effect) raises the multiphase strength in about 165 to 176 MPa, almost independently of both M-content (16 % to 2 % respectively) and M-strength. Therefore, in order to increase DP strength the refinement of the structure is more effective than alloying to produce harder Martensite, particularly at the low M-contents.

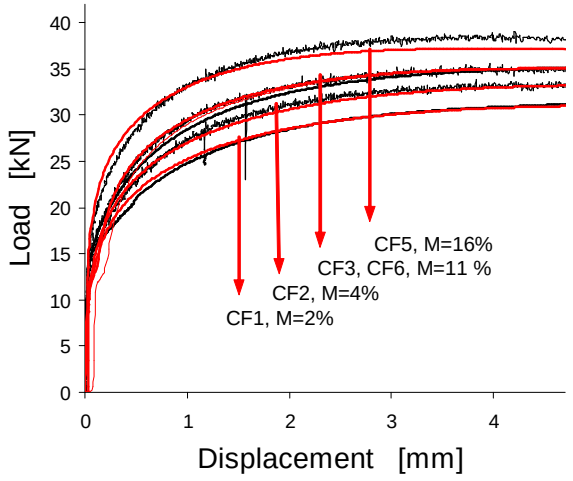

Figure 9: Validation of SCS-m model simulation results against raw experimental data.

Figure 9 shows the result of a more severe validation of the simulations against the raw load-displacement data for the quasi-static testing.

4 Modelling higher strain rate testing

Even though the maximum strain rate achieved in the experiments (about 4 s-1) is still low for impact applications, it is five orders of magnitude higher than in the quasi-static testing in §3. Also, in contrast with ballistic speeds [17], there are minimal dynamic effects, factor which is important to extract only the constitutive response required as input in the FEM analysis. Figure 5b shows the combined effects of strain rate and M-content on the strength factor K and strain hardening coefficient n in the Swift relationship $\sigma = K(\varepsilon - \varepsilon_o)^n$. It can be seen that although the strain rate is the predominant parameter, the influence of M-content in the range explored cannot be neglected.

4.1 Rate dependent enhanced SCS-m model

The empirical correlations for the constitutive coefficients in Figure 5b were extrapolated to zero M-content and then used to scale the quasi-static Ferrite behaviour from the reference strain rate $\dot{\varepsilon}_o$ to any new higher strain rate $\dot{\varepsilon}$ (T4.4 in Table 4). Figure 10a compares the experimental true strain-true stress results for cylindrical specimens against the simulations produced with the enhanced **SCS-m**, at 2 M-contents and 3 strain rates. The fitting in the ranges of M-content 2 to 11 %, strain rates 0.00024 to 3.8 s^{-1} and up to the uniform strain limit is good.

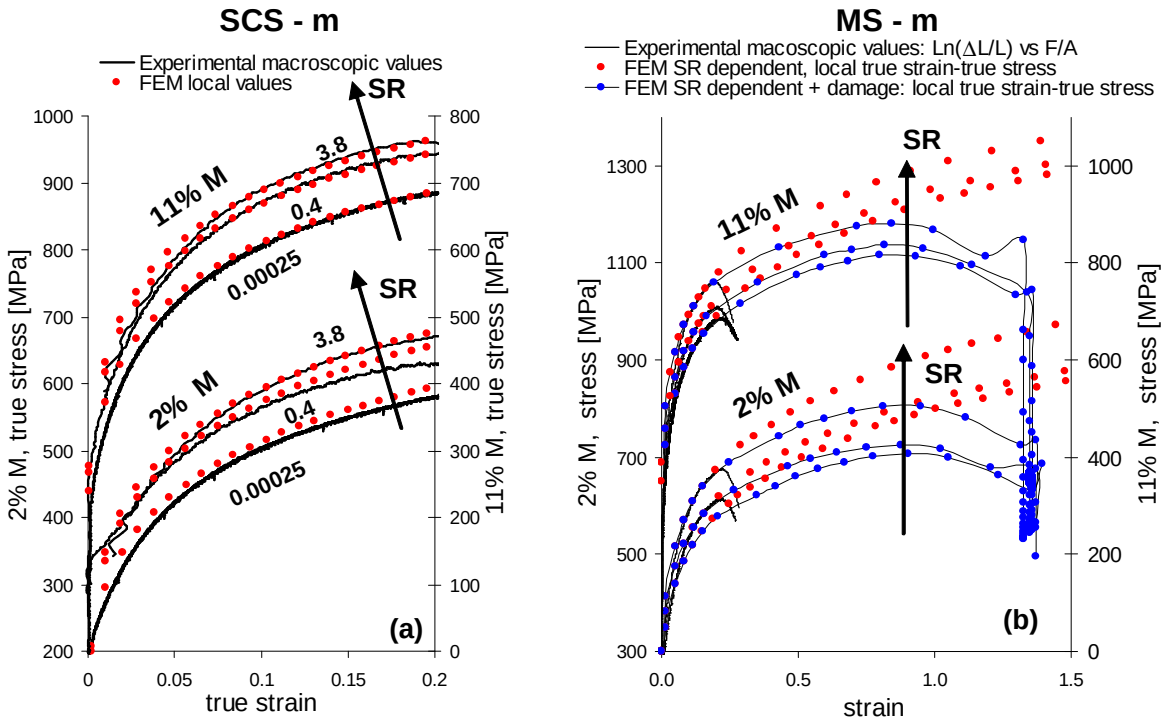

Figure 10: Comparison of experimental (macroscopic) vs. FEM local (specimen center) strain-stress results. Unnotched cylindrical specimen, 9 mm diameter, 2 M-contents and 3 strain rates (a) **SCS-m** model, (b) **MS-m**; L and A are the current specimen dimensions.

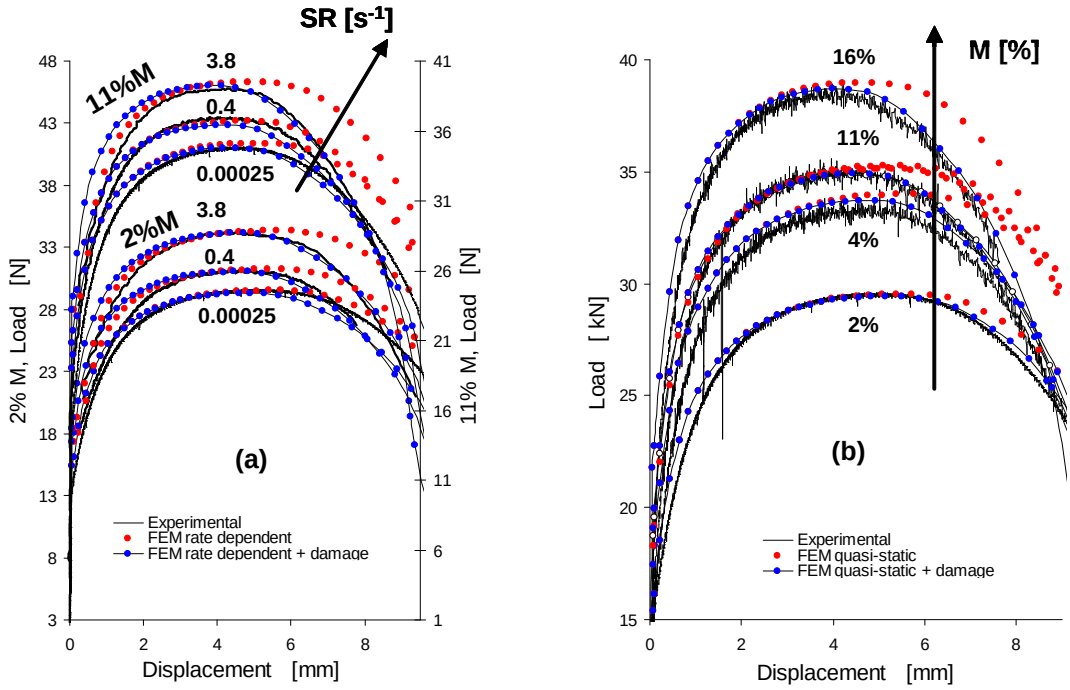

Figure 11: Comparison of raw load-displacement experimental results and **MS-m** simulations with and without damage at: (a) 3 strain rates and 2 M-contents; (b) 4 M-contents at quasistatic conditions. Cylindrical specimen, 9 mm diameter.

4.2 Rate dependent MS-m model based on multiphase strain and incorporating damage

A strain hardening **MS-m** model (T4.5 in Table 4) in terms of the macroscopic total strain up to the uniform deformation limit was built up from the correlations found at quasi-static conditions for the several M-contents in the series CF's (Figure 5a). For rate-dependent applications, the multiphase stress level was scaled by the factor obtained from the strain rate testing given in Figure 5b. A comparison of the experimental and simulation results in terms of strain-stress is shown in Figure 10b.

The **MS-m** was next upgraded coupling the above strain hardening model to the damage formulation due to Gurson [13-14] (T4.6 in Table 4). In this model the void volume fraction rate is written as the sum of nucleation and growth contributions; the first one evolves with the strain from a Gaussian distribution centred on a nucleation strain ε_N, computed from the uniform strain limit determined from the tensile testing experiments.

The true stress-true strain predictions from this rate dependent model enhanced with damage are superposed to both the compact solid simulations and experimental results in Figure 10b. The key calibration feature is that the FEM damaged stress results for large strains in Figure 10b correspond to the best fitting against the experimental raw load-displacement data in the same set of simulations (Figure 11a). The stress difference between the two FEM simulations (compact vs. damaged solid) in Figure 10b gives a quantification of the effects of damage for strains beyond the uniform deformation limit up to nearly fracture. The stress overshoot prior to collapse in Figure 9b is a numerical problem and its contribution to the total internal work is negligible. The model fails to reproduce the last stage of fracture, but nevertheless gives good prediction during the nucleation and early growth stages of failure. Figure 11b shows the application of the same **MS-m** modelling to the experimental testing in §3 for the several M-contents of series CF's at a common quasi-static strain rate. The objective of this task was to obtain improved large strain-stress results and hence toughness values for its correlations to the multiphase structure parameters.

5 Tensile toughness-microstructure relationships

A measure of tensile toughness is given by the amount of internal plastic work [16]:

$$C_1 = \Delta E = \int \sigma . d\varepsilon \tag{2}$$

or specific energy absorbed by the material up to nearly its fracture, called toughness modulus by some authors. The computation of this parameter using the experimental engineering macroscopic strain gives values too small and without a very definite trend (Figure 12a), because such strain measure is no longer representative as triaxiality develops with necking. The alternative given by FEM large deformation analysis incorporating rate dependent effects and material degradation (§4.2), provides a more reliable large strain measure beyond the strain to peak stress. Figure 12 shows the behaviour of this toughness modulus in terms of testing strain rate and microstructural parameters:

(a) Toughness increases with the testing speed at a rate that is higher when the M-content is lower (Figure 12a, sample CF1, M=2 %).

(b) Toughness at quasi-static conditions shows low sensitivity to M-content (Figure 12b)

(c) Toughness worsens with the coarsening of the structure, and its sensitivity is almost one order of magnitude higher to d_M than to the FGS. (Figure 12c).

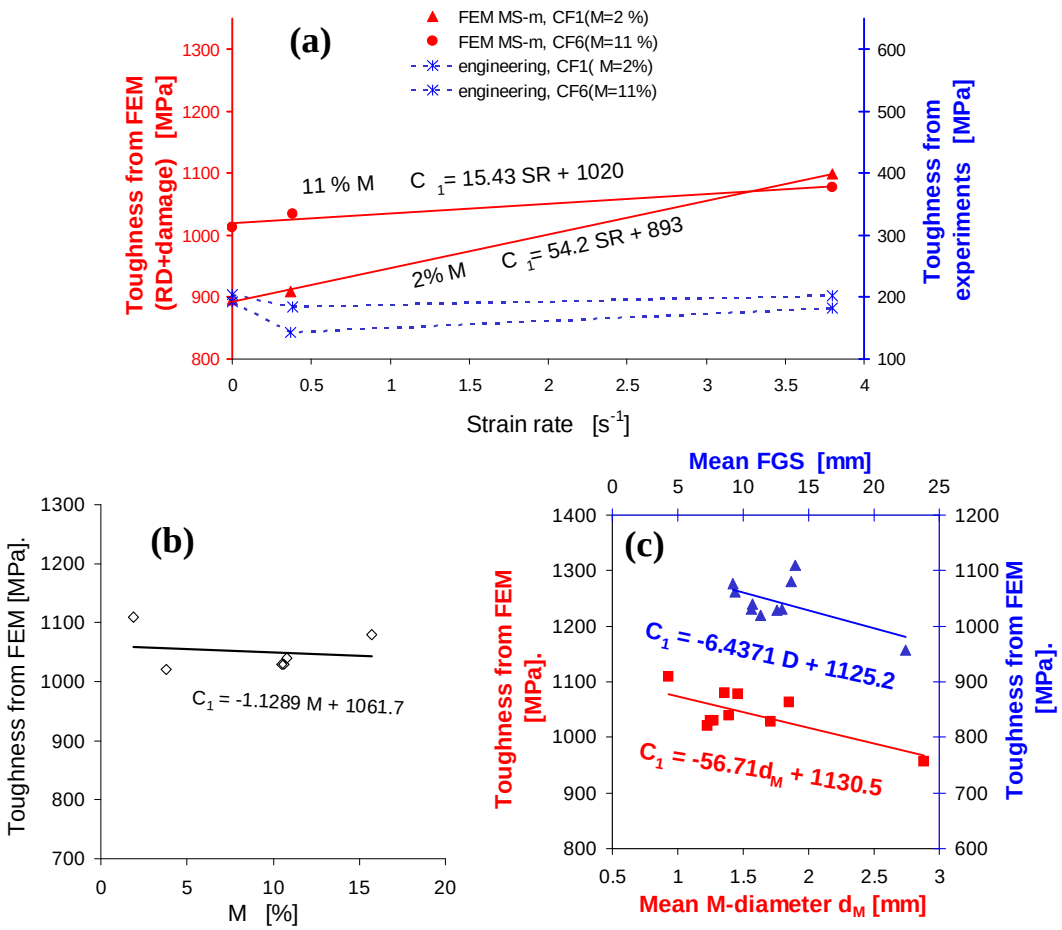

Figure 12 FEM simulation results for tensile toughness from MS-m model for CSM testing in terms of microstructural parameters and strain rate.

6 Overall conclusions

(a) A pre-treatment by reheating above Ac3 followed by fast quenching was important to the structure resulting in the following intercritical annealing. Dual phase steels with M-content from 2% to 16%, FGS 9 to 22 microns and d_M 0.9 to 2.9 microns were produced from the original F-P structures and used in the mechanical testing.

(b) The tensile properties strength Rm, strain to fracture and toughness are about one order of magnitude more sensitive to the size of the Martensite islands than to the FGS; Rp02 increases with d_M at 10.7 [MPa/microns] while Rm decreases at 14.5 [MPa/microns].

(c) Rp02 increases with the M-content in 4 [MPa / %M] while Rm increases at 7.1 [MPa/ %M].

(d) Higher Rm/Rp02 ratios results for small d_M, small FGS and low M-contents, factors these not necessarily achieved in the same annealing.

(e) Two continuous models: **SCS-m** and **MS-m** to predict strain-stress behaviour of dual phase F-M steels have been developed and interfaced as elastoplastic materials to a FEM platform [14]. The Self-Consistent Strain model **SCS-m** is the extension of previous work to higher strain rates, uses a strain partition, incorporates size effects via a Multiphase Interaction Stress related to microstructural parameters and is valid up to the uniform strain. **MS-m** is based on the multiphase strain, incorporates both rate effects and damage nucleation and growth, it is valid for large strains almost up to fracture and was used to produce a measure of tensile toughness. **MS-m** can be merged in a future in the framework of the **SCS-m**. The predictions have been validated against experimental results involving a span of five orders of magnitude in strain rate with good agreement.

(f) Given the good matching to raw results in Figure 11, an estimation of the variability of tensile properties predictions can be drawn from their experimental sensitivities to microstructural parameters (b) and (c) above and the uncertainty in the determinations of these as quantified by the standard deviation in Table 3. This gives Rp02 spreading values in MPa from 0.9 to 3.8

due to M content, 4.5 to 8.0 due to FGS and 1.71 to 7.6 due to d_M ; Rm spread values in MPa vary from 1.7 to 6.8 due to M content, -3.1 to -5.5 due to FGS and -2.3 to -10.3 due to d_M .

(g) Although validated here for uniaxial tension the models developed in this framework are suitable to be extended after appropriate validations, to complex loading situations as those resulting in dynamic loading and cold metal forming.

7 References

[1] Parker S., Wadsworth J.E., Gutierrez I., Rodriguez Ibabe J.M., Vandenberghe L. and Lotter U., 'Property models for mixed microstructures', *Technical Steel Research, Final Report N° EUR 20880*, ISBN: 92-894-6255-8, Office for Official Publ. of the E.U.(2003).

[2] Gutierrez I., Parker S.V., Bianchi J. H., Paul G., Mesplont C., Wojcicki M., Altuna M. A., Vescovo P., Kawalla R. RFCS Project contracts RFS-PR-02013, 'Mechanical Property Models for High Strength Complex Microstructures (MEPMO)'. *Technical Steel Research*, *Final Report.* Office for Official Publ. of the E.U. (2007) *in press*.

[3] Buessler P., Bouaziz O., Iung T., Gil Sevillano J., Vrieze J., Kaluza W., Esnaola J.M., Bonifaz E., Meizoso A., 'Modelling of mechanical properties and local deformation of high strength multi-phase steels'. *Technical Steel Research, Final Report N° EUR 20331 ,* ISBN 92-894-3660-3, Office for Official Publ. of the E.U. (2002).

[4] Fleck, N A ; Muller, G M ; Ashby, M F ; Hutchinson, J W , 'Strain gradient plasticity: theory and experiment', *Acta Met. et Mat.* 42, (2), Feb. 1994, pp. 475-487

[5] Bouaziz O., Iung T., Kandel M. and Lecomte C., 'Physical modelling of microstructure and mechanical properties of dual phase steel', *J. Phys. IV*, France 11 (2001), EUROMECH-MECAMAT'2000, EDP Sciences, Les Ulis, 224-231.

[6] Perlade A., Bouaziz O.,Furnemont Q., 'A physically based model for TRIP-aided carbon steel behaviour', *Mat. Sci. and Eng.*, A356 (2003) 145-152.

[7] Bouaziz O., Buessler P.; Mechanical behaviour of multiphase materials: an intermediate mixture law without fitting parameter, *Rev. Met.* 99 (2002) vol. 1; 71-77

[8] Stringfellow, R. G., Parks D.,'A self-consistent model of isotropic viscoplastic behaviour in multiphase materials', *Int. J. Plasticity*, 7, pp. 529-547 (1991).

[9] Rudiono, Tomota Y., 'Application of the secant method to prediction of flow curves in multi-microstructure steels', *Act. Mat*., 5 (1997) 1923-1929.

[10] Tomota Y., Umemoto M., Komatsubara N, Hiramatsu A., Nakajima N., Moriya A., Watanabe T. Nanba S., Anan G., Kunishige K., Higo Y. and Miyahara M., 'Prediction of mechanical properties of multi-phase steels based on stress-strain curves', *ISIJ Int*. ,32 (1992) 343-353.

[11] Sellger R., Bianchi J.H., Hoglund L., Hillert M., Agren J., 'Control of phase transformation during processing of partially bainitic multi-component strip steels for controlling the work-hardening characteristics. *Technical Steel Research, Final Report N° EUR 20582* , ISBN 92-894-5153-X, Office for Official Publ. of the E.U. (2003).

[12] Bianchi J, 'Prediction of mechanical properties of partially bainitic multiphase steel strip' , Proceedings of the Joint ECSC-Nest Workshop. Advanced Hot Rolling Practice and Products', 5-6 October 2000, VDEh, Dusseldorf, 11 pages, J. Ball editor, published in CD-ROM by *DG Research, ECSC Steel RTD programme*, ISBN 92-894-1356-5.

[13] Gurson, A. L.,'Continuum Theory of Ductile Rupture by Void Nucleation and Growth: Part I—Yield Criteria and Flow Rules for Porous Ductile Materials', *Journal of Engineering Materials and Technology*, vol. 99, 1977, 2–15.

[14] ABAQUS ®, *User's Manuals*, 2002-2007.

[15] Grujicic M., Erturk T., Owen W., 'A finite element analysis of the effect of accomodation strains in the ferrite phase on the work hardening of a dual phase steel', *Mat. Sc. and Eng*., 82 (1986), 151-159.

[16] Masaaki Itabashi, Kozo Kawata, 'Carbon content effects on High strain rate tensile properties for C-steels, *Int. Journal of Impact Engineering,* 2000, 24(2) 117-131.

[17] Wong C. IISI-AutoCo Round-Robin Dynamic Tensile Testing Project, *International Iron and Steel Institute*, 2005.